High dynamic range streak camera for subpicosecond time-resolved x-ray spectroscopy

C. Bonté, M. Harmand, F. Dorchies, S. Magnan, V. Pitre, J.-C. Kieffer, P. Audebert, and J.-P. Geindre

Articles you may be interested in

Time-resolved soft x-ray spectra from laser-produced Cu plasmaa)
Rev. Sci. Instrum. **83**, 10E138 (2012); 10.1063/1.4739071

Streaked x-ray spectrometer having a discrete selection of Bragg geometries for Omegaa)
Rev. Sci. Instrum. **83**, 10E107 (2012); 10.1063/1.4729501

Twin-elliptical-crystal time- and space-resolved soft x-ray spectrometer
Rev. Sci. Instrum. **77**, 10F315 (2006); 10.1063/1.2227444

Temporal resolved x-ray penumbral imaging technique using heuristic image reconstruction procedure and wide dynamic range x-ray streak camera
Rev. Sci. Instrum. **75**, 4010 (2004); 10.1063/1.1787900

Conical x-ray crystal spectrometer for time integrated and time resolved measurements
Rev. Sci. Instrum. **74**, 2369 (2003); 10.1063/1.1556953

High dynamic range streak camera for subpicosecond time-resolved x-ray spectroscopy

C. Bonté, M. Harmand, and F. Dorchies[a)]
Université Bordeaux I, CNRS, CEA, CELIA UMR 5107, 351 cours de la Libération, Talence, F-33405 France

S. Magnan, V. Pitre, and J.-C. Kieffer
I.N.R.S.-Énergie, Matériaux et Télécommunications, 1650 boul. Lionel-Boulet, Varennes, Qc, J3X 1S2, Canada

P. Audebert and J.-P. Geindre
Laboratoire pour l'Utilisation des Lasers Intenses (LULI), École Polytechnique, 91128 Palaiseau, France

The full characterization of a time resolved x-ray spectrometer is presented. It is based on the coupling of a conical crystal with a subpicosecond x-ray streak camera. The detector is designed to operate in accumulation mode at high repetition rate (up to 1 kHz) allowing signal to noise ratio as high as $10^4:1$. Optical switches have been used to limit the jitter induced in the subpicosecond range, demonstrating the very long term stability (a few hours) of the entire device. The data analysis have been developed to get the spectral and temporal resolution of an ultrashort laser-plasma-based x-ray source. © *2007 American Institute of Physics.* [DOI: 10.1063/1.2720718]

I. INTRODUCTION

With the advent of short and intense laser pulses, new ways for hot and dense plasma generation are being investigated. Fundamental interests stimulate the characterization of the emitted x rays, say as information on ionization or electronic temperature and density. Further interest lies in characterizing such plasmas as potential ultrashort x-ray sources. In this context, it is challenging to get high resolution spectra together with subpicosecond time resolution and a dynamic range as high as possible.

Two different approaches have been considered to get temporal resolution. An indirect method consists in the cross correlation between the x-ray emission and an ultra fast physical process. This last is excited by a "pump" laser pulse obtained from the main laser pulse with a beamsplitter, while the "probe" drives the x-ray emission. This "pump and probe" method has been successfully employed with different physical processes in the subpicosecond range[1–6] and the temporal resolution may be down to a few 100 fs. Nevertheless, these proposed techniques require a specific setup and give information only for a predetermined x-ray wavelength. An alternative method consists in measuring directly the x-ray spectrum with a temporal resolution. For this purpose, the emission is spectrally dispersed by a crystal. The temporal resolution is then achieved with the help of an x-ray streak camera.

Picosecond and subpicosecond resolution streak camera have been developed for a decade.[7–10] Coupling a streak camera together with an x-ray crystal has been realized for different crystal configuration.[11–14] However, most of the presented works are realized in single shot mode, and are limited to a signal to noise ratio (SNR) as low as 10:1,

mainly due to the space charge effect.[15] Another study has been presented,[16] demonstrating close to 250 fs resolution in accumulation mode. This value is obtained with a 5 μm slit in the x-ray tube, drastically reducing the detection efficiency. The major challenge is to provide good SNR spectra together with a subpicosecond resolution. In accumulation mode, one may expect such a dynamic range.[12] Lowering the detection threshold and massively accumulating seem to be a reasonable way to get high dynamic range time-resolved spectra. Accumulation mode creates residual jitter, which depends a lot on the temporal stability of the laser. This jitter drastically reduces the effective temporal resolution achievable. One solution to limit such a jitter is based on optical switches.[17,18]

In this article, we report the extended characterization of a high dynamic range x-ray time resolved spectrometer based on an x-ray streak camera. The tube properties (e.g., focusing and curvatures), its spatial resolution, and the temporal resolution are presented. We pay special attention to the long term stability due to the temporal jitter. The study of the dynamic range is presented and the mechanism of saturation and the detection threshold are detailed. The coupling with a conical crystal to get x-ray time-resolved spectroscopy is presented. A typical x-ray time-resolved spectrum obtained is shortly presented, together with the experimental image analysis method.

II. DESCRIPTION OF THE DETECTION SYSTEM

We present in Fig. 1 the layout of our detection system. An x-ray source is issued from laser-matter interaction. A conical crystal is used to disperse and focus the x-ray spectra along a line, perpendicular to the detection axis. The focusing is adjusted along the entrance slit of the streak camera thanks to motorized translating plates (not presented for clar-

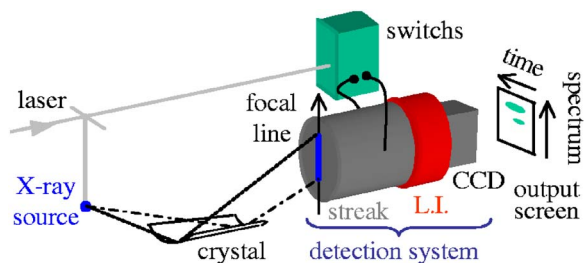a)Electronic mail: dorchies@celia.u-bordeaux1.fr

FIG. 1. (Color online). Sketch of the ultrafast detection system. A conical crystal is coupled with a streak camera, whose sweeping plates are triggered with a part of the main laser pulse thanks to optical switches. A LI can be inserted between the streak tube phosphor screen and a CCD camera. On the right, the temporal and spectral axis are indicated on the recorded image.

ity reasons). Sweeping plates are triggered thanks to optical switches with the use of a "trigger" laser pulse which is obtained from the main laser pulse behind a beamsplitter. The streaked signal can then be amplified with a light intensifier (LI), before being detected using a charge-coupled device (CCD). The streak tube and the optical switches, respectively, have been developed by Photonis (bilammelar P863X/D1 tube) and Fastlite corporations. The CCD camera is a 1340×1300 imaging array from Princeton Instruments with $20 \ \mu m$ pixel size, and six visible photons per CCD count sensibility (including the quantum detection efficiency), with stabilized temperature at $-35 \ °C$. We express some results afterwards in term of pixel and CCD counts for convenience.

We look forward an extended characterization in order to quantify the spectral and the temporal resolutions, the dynamic range, and the detection efficiency. The temporal resolution, for instance, depends on the extracting field on the photocathode, on the focusing on the temporal axis, on the sweep speed, on the spatial resolution of the read-out system, and on the jitter, which are related respectively to the streak camera, the CCD camera, and the optical switches. Therefore, each element of our detection system has been studied independently, with the use of ultraviolet (UV) and x-ray ultrashort sources:

- the tube streak (having incidence on the spatial and temporal resolutions),
- optical switches (limiting the temporal resolution in accumulation mode),
- the light intensifier and the CCD camera (contributing to the dynamical range), and
- the crystal (responsible for the spectral dispersion).

The whole setup has been successfully implemented on a laser-cluster interaction experiment, as shown at the end of this article.

III. SPATIAL AND TEMPORAL CHARACTERIZATION

A. Experimental setup

The spatial and temporal properties of the presented ultrafast detection system mainly depend on the streak tube. Its principle of operation is briefly reminded. X-ray photons are converted into electrons through a photocathode placed at the entrance of the streak tube. A high static voltage (called
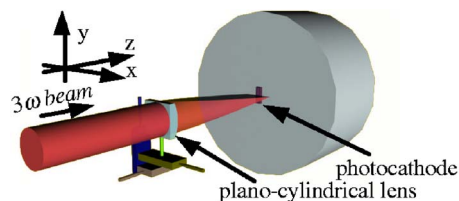

FIG. 2. (Color online). Sketch of a part of the experimental setup devoted to the streak camera characterization with UV pulses.

V_{PK} later) is applied between the photocathode and an accelerating slit. Electrons are extracted and projected onto a phosphor screen at the output of the tube. Electrostatic lenses ensure the electrons focusing, leading to a thin trace on the screen. This trace can be temporally swept using a fast-varying electric field, with direction perpendicular to the accelerating slit.

A full characterization has been realized with the CELIA kHz laser. This last is based on chirp pulse amplification technique and Ti:sapphire crystals.[19] It delivers up to 10 mJ laser pulses, centered at 805 nm, and with pulse duration down to 40 fs full width at half maximum (FWHM). The results indicated in this section are mainly obtained with an UV source, realized by frequency tripling the fundamental wavelength (3ω) with two non linear crystals (200 μm thickness BBO). The 3ω wavelength (268 nm) is in the sensible domain of the streak camera and UV pulses are sufficiently short[20] to determine the temporal resolution of the streak camera.

The experimental setup is partly presented in Fig. 2. We used a planocylindrical lens with a spatial focusing control ensured by three-axis plate translations and one rotation mount (not shown for clarity). A vacuum chamber (not presented in Fig. 2) is set up at the entrance of the streak camera in order to reach high extracting electric field on the photocathode. A pressure of 10^{-5} mbar is low enough to reach fields up to 100 kV/cm. The pressure separation and the light propagation at 3ω is ensured by a synthetic quartz glass (suprasil) window. For operation with x rays, a 25 μm Be filter fulfills these two conditions. A Palladium photocathode is used for UV source, and KI photocathode for x-ray source. The spatial performances of the detector do not depend on the photocathode used. But that plays a significant role for the temporal resolution.

B. Tube imagery

1. Spatial resolution

The spatial resolution is usually measured applying grids on the photocathode, with different spatial frequencies and measuring the subsequent contrast transfer function (CTF).[21] The scheme presented in Fig. 2 is an alternative and easier way to get the spatial resolution. The UV is focused along the x axis perpendicular to the entrance slit (y axis). The width of the UV signal is measured when directly focused onto a CCD: $30 \pm 5 \ \mu m$ FWHM. It is then compared with the width recorded at the output of the streak camera. The static voltages applied on the streak tube electrodes were set at the values that optimize both the focusing along the spatial and
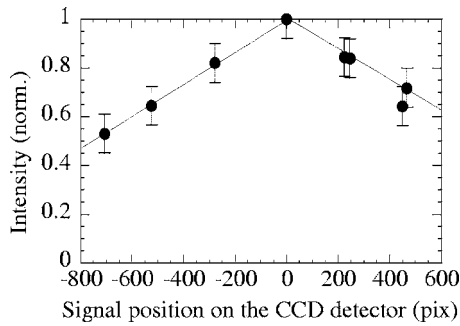
FIG. 3. Intensity of the signal recorded on the CCD at the streak output (normalized to the maximum) as a function of the position along the temporal axis.
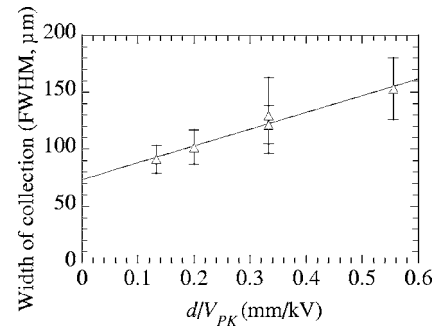

FIG. 4. Width of the collection surface as a function of the inverse of the extracting field. Empty triangles: experiment. Full line: linear fit.

the temporal axis. From these measurements we have determined the best spatial resolution: 32 ± 9 μm FWHM. That corresponds to a CTF=50% for a grid with 16 ± 4 lp/mm. A degradation is observed when the sweeping voltage is applied. Thus, the effective best spatial resolution becomes 49 ± 9 μm FWHM. It is observed to be homogeneous along the two axis of the screen.

The magnification is obtained with the same setup, displacing the UV incident line along the streak entrance slit (y axis). Its value is -1.85 ± 0.01.

2. Homogeneity

The homogeneity of the camera streak response has been studied on both temporal and spatial axis. First, the input signal is focused along the y axis. The signal conversion has been observed to be uniform all along this spatial axis, with fluctuations below 10%. Since photocathodes are usually very hygroscopic, this should be checked before any operation. Then, the output signal is shifted applying different static voltages on the sweeping plates. The incident signal intensity is kept constant. The recorded intensity is presented in Fig. 3 as a function of the position along the temporal axis. The origin is set to the symmetry axis of the streak tube. The measured signal is maximum on this axis and linearly decreases down to 50% near the edges of the output screen. This effect is due to the internal tube design and it should be considered for experimental analysis.

3. Collection surface on the photocathode

The collection surface at the entrance of the streak tube is delimited: (i) along the y axis by the length of the accelerating slit (15 mm) and (ii) along the x axis by a width to be determined. This last part depends on the accelerating slit aperture (1 mm in our case). It is an important issue since x-ray spectra have to be focused into that "window." The collection width has been determined with the experimental setup described earlier (cf. Fig. 2). The UV signal is focused along a line parallel to the entrance slit (y axis). The output signal intensity is recorded as a function of the focal line position, which is scanned in the transverse direction (along the x axis). From these measurements, we determine the collection width. Its value is reported in Fig. 4 as a function of the inverse of the extracting field. Different values of the extracting voltage V_{PK} and distance d from the accelerating

slit to the photocathode have been considered. The behavior is found to be linear, and the width is 93 ± 10 μm for our usual conditions ($V_{PK}=15$ kV and $d=2$ mm). The collection width is observed to decrease with an increasing extracting field. That is coherent with results reported by Jaanimagi[22] on virtual cathode.

4. Traces curvatures

The streaked trace has a parabolic shape on the release screen, both in static and dynamic mode, as shown in Fig. 5. The top of Fig. 5 shows different output traces recorded on the CCD with application of different static bias voltage V_b on the sweeping plates. The signal is slightly curved along the temporal axis. We define the static curvature strength (CS_{stat}) to be the coefficient of the squared component of a second order polynomial fit. It is found to be proportional to the distance P from the trace to the tube symmetry axis. Expressed in pix/pix^2 on the CCD camera, $CS_{stat} = (7.1 \pm 0.1) \times 10^{-8} P(\mathrm{pix})$.

In dynamic mode, an additional component of the trace curvature is due to the differential path length of the electrons emitted from the photocathode along the y axis. That leads to a differential temporal delay when impacting the phosphor screen. The bottom of Fig. 5 shows output traces recorded with different delay between the incident UV pulse and the trigger pulse on the optical switches. An additional curvature CS_{dyn} is observed. Its strength is found to be related to the extracting voltage V_{PK} and to the sweeping voltage amplitude V_{tot} (both expressed in volts), according to the following relation: $CS_{dyn}(\mathrm{pix/pix}^2)=(8.7 \pm 0.2) \times 10^{-2} V_{tot}/V_{PK}^{3/2}$. A simple consideration of linear trajectories for the electrons from the photocathode to the phosphor
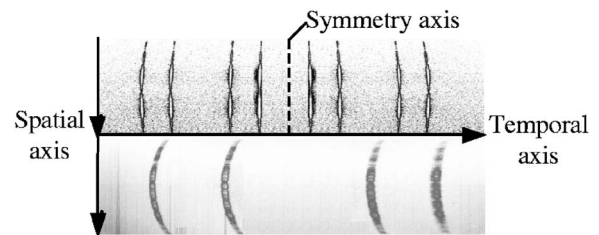

FIG. 5. Static and dynamic curvatures. Top image: Various traces are reported for different bias voltage V_b, without any sweeping (static mode). The central dashed line indicates the symmetry axis of the streak tube. Bottom image: The same trace is swept (dynamic mode) and reported with various time delay between the sweeping and the UV input pulse.
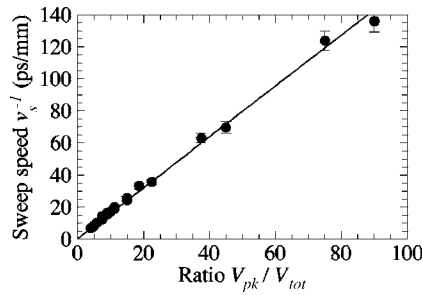
FIG. 6. Sweep speed as a function of the ratio V_{PK}/V_{tot}. The solid line is the corresponding linear fit.

FIG. 7. Temporal width of the streaked trace as a function of the extracting voltage V_{PK} with a distance $d=2$ mm between the photocathode and the extracting slit. Different lines detail the different contributions to the temporal resolution.

screen leads to such an analytical dependence on the applied voltages. Taking account of these curvatures, an automatic image processing is performed, within a temporal uncertainty of 1 ps all along the corrected streaked signal.

C. Temporal resolution

The temporal resolution Δt is considered to be the quadratic sum of different components as follows:[15]

$$\Delta t^2 = \Delta t_{LSF}^2 + \Delta t_{PK}^2 + \Delta t_{SC}^2 + \Delta t_{jitter}^2, \tag{1}$$

where Δt_{LSF} is due to the line spread function (i.e., the ability of the tube to focus the trace), Δt_{PK} is due to the photocathode-induced dispersion, Δt_{SC} is due to the space charge effect inside the tube, and Δt_{jitter} is due to the temporal erratic sweeping. The UV pulse duration Δt_{signal} used in our setup is estimated to be less than 50 fs root-mean-square[20] (rms) and has therefore no significant effect on the temporal characterization presented therein.

The focused signal width on the output screen of the streak camera along the temporal axis is called the line spread function. In order to determine it with a good spatial resolution, a fiber optic taper, with a magnification factor of 2, has been introduced between the streak tube phosphor screen and the CCD camera. Without voltage on the sweeping plates, the static trace width is measured to be 37 ± 6 μm FWHM. Following the previous comment made in Sec. III B 1 the sweeping voltage should degrade this value, leading to an effective value of LSF$=52\pm7$ μm FWHM. Contribution of the LSF to the temporal resolution is given by $\Delta t_{LSF}=v_s^{-1}\times$LSF, where v_s is the sweep speed. Figure 6 shows the inverse of the sweep speed v_s^{-1} as measured as a function of the ratio V_{PK}/V_{tot}. Measurements follow the relation: v_s^{-1}(ps/mm)$=(1.7\pm0.1)\times V_{PK}/V_{tot}$. This linear dependence may be easily found, considering the trajectory of a photoelectron accelerated by the extraction voltage V_{PK} and deflected by the sweeping electric field related to V_{tot}. The coefficient magnitude mainly depends on the tube geometry. With our usual experimental conditions ($V_{PK}=15$ kV and $V_{tot}=2$ kV), we get $\Delta t_{LSF}=660\pm140$ fs FWHM, that is 280 ± 60 fs rms.

Photocathodes are designed to optimize the yield of secondary electrons at their rear surface. These electrons have a Lambertian angular distribution:[23,24] the number of electrons emitted with an angle θ, related to the tube axis, is proportional to $\cos(\theta)$. Their energetic distribution is proportional to $q_eV_0/(q_eV_0+W)^4$, where q_eV_0 is the initial kinetic electron
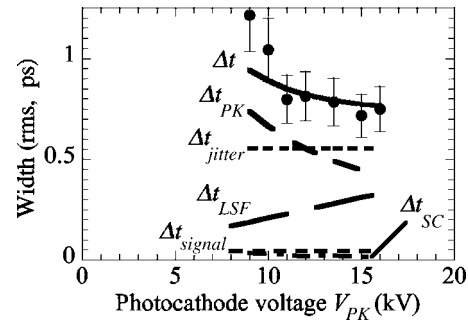
energy and W is a constant depending on the material (1.1 eV for KBr, 0.61 eV for KI).[23] A temporal dispersion Δt_{PK} $\propto\sqrt{W\times d/V_{PK}}$ is induced between the photocathode and the accelerating slit.[25] There is a little additional contribution when the electrons fly from the accelerating slit to the phosphor screen.[26] The highest extracting fields are required in order to minimize the total temporal dispersion. This effect depends on the photocathode material. It has been calculated for KI and KBr photocathodes, usually used in x-ray studies.[22] For our day-to-day running conditions (KI photocathode), it is expected to have a contribution of Δt_{PK} $=260$ fs rms. Our characterization with UV pulses has been realized with a Palladium photocathode. Without available data on Palladium W parameter, the corresponding value $\Delta t_{PK}=430$ fs rms has been deduced from the total temporal resolution.

The space charge effect enlarges the trace width at the streak tube output, and therefore deteriorates the temporal resolution. A specific attention has been paid to this effect, which is related to the number of electrons in the tube (cf. Sec. IV C thereafter), Concerning the results presented here, the input signal level is low enough so that no significant incidence is expected on the total temporal resolution.

In accumulation mode, a new component Δt_{jitter} contributes to the total temporal resolution, issued from the temporal erraticity between the sweep trigger and the incident signal. This temporal jitter leads to a shot to shot shift of the trace temporal position on the streak tube output screen. In order to control this effect, the trigger of the sweeping voltage is ensured by optical switches, whose resistivity is sensitive to an incoming laser pulse synchronized with the main laser pulse. A residual jitter remains, due to the shot to shot laser energy fluctuation. It can be decreased, by increasing the laser energy, in order to saturate the optical switches. Nevertheless, if the laser pulse is too energetic, the amount of energy in the pedestal (attributed to amplified spontaneous emission) can be high enough to trig the sweeping voltage. In order to minimize the jitter under these two constraints,[8,18,27,28] the laser energy on optical switches has been set to a value greater than 50 μJ and the pulse is actively filtered with a 2 mm RG filter (saturable absorber).

The temporal width of the streaked trace obtained with the best conditions is presented in Fig. 7 as a function of the extracting voltage V_{PK}, together with its different contribu-
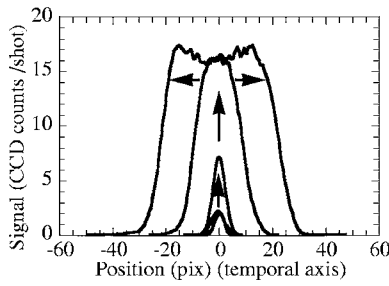
FIG. 8. Temporal profile of streaked traces measured with different incident intensities and $V_{PK}=15$ kV. Arrows indicate the evolution corresponding to increasing incident UV pulse energy.

tions. In order to avoid electric arc, V_{PK} does not exceed 15 kV in routine conditions. In that case, the temporal resolution is estimated to be $\Delta t=770\pm130$ fs rms for accumulation over more than 10^3 shots. We can easily see on the figure that it is mainly limited by the jitter $\Delta t_{\text{jitter}}=560\pm90$ fs rms.

IV. DYNAMIC RANGE

A. Space charge effect and photocathode saturation

Different trace profiles along the temporal axis are presented in Fig. 8 with $V_{PK}=15$ kV. A Gaussian shape is observed for low energy incident UV pulse. When the UV energy increases, the recorded signal grows and then saturates and broadens. This observation is understood as the space charge effect between the electrons in the tube, along the temporal axis. Studies indicate that the temporal broadening Δt_{SC} is proportional to the number of electrons N_e per bunch inside the streak camera.[29–31] Qian et al.[32] suggest the following relation:

$$\Delta t_{\text{SC}} = \frac{\sqrt{q_e m_e}L^2}{4\sqrt{2}\pi\varepsilon_0}\frac{N_e}{r_{eq}^2 V_{PK}^{3/2}}, \qquad (2)$$

where m_e is the rest mass of an electron, L is the tube length, r_{eq} is the radius of the electron beam, and ε_0 is the vacuum permittivity. The temporal broadening measured is reported for different extracting voltages in Fig. 9, as a function of the time-integrated output signal. As expected from Eq. (2), a linear behavior is observed with the output signal intensity, i.e., with the number of electrons inside the streak tube. This effect is very sensitive to the electron velocity inside the streak tube, i.e., to V_{PK}. That confirms the necessity to operate with the highest extraction voltage.
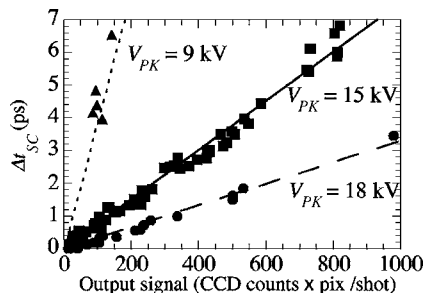

FIG. 9. Temporal broadening Δt_{SC} due to the space charge effect as a function of the time-integrated output signal. Dotted, full, and dashed lines are linear fits of experimental data recorded at 9, 15, and 18 kV, respectively.
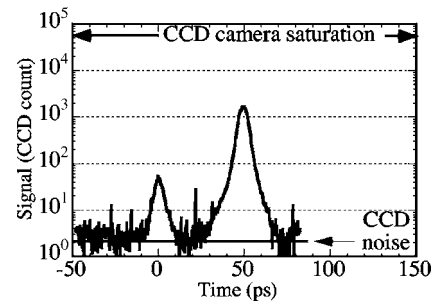

FIG. 10. Measurement of two UV pulses separated by 50 ps, in accumulation mode (10^3 shots).

Saturation effect could occur at the photocathode for intense incident signal,[33] leading to a limiting Child–Langmuir current density J_{CL},

$$J_{\text{CL}}(\text{A cm}^{-2}) = \frac{4\varepsilon_0}{9}\sqrt{\frac{2q_e}{m_e}}\frac{V_{PK}^{3/2}}{d^2}. \qquad (3)$$

With our usual operating conditions ($V_{PK}=15$ kV and $d=2$ mm), the current density saturation is around 100 A/cm^2, which is three orders of magnitude greater than the threshold leading to a space charge effect as important as the photocathode-induced temporal dispersion. The output signal has been measured and integrated over the temporal axis as a function of the incident UV pulse energy. A linear behavior has been observed up to an incident energy two orders of magnitude higher than the threshold level defined just before. As the incident signal is usually chosen to be low enough to prevent from the space charge effect, the saturation may be also neglected.

B. Signal to noise measurement

The upper limit of the dynamic range is related to the 16 bit CCD camera ($\sim$60 000 counts). Let us consider now the lower limit of this dynamic range. When a single photoelectron impacts the output phosphor screen, approximately 800 photons are recorded on the CCD camera, spreading over the zone corresponding to the spatial and temporal resolution ($\sim$20 pix^2). That limits the signal magnitude to six counts per pixel. The thermal noise of the CCD evolves like the square-root of the exposure time and for 900 s acquisition duration ($\sim$10^6 accumulated shots), the noise corresponds to 25 CCD counts. The analysis of these data allows an average on a few pixel rows and columns within the spatial and temporal resolution. That subsequently reduces the CCD noise influence. We present in Fig. 10 an example of the signal to noise ratio that could be reached. Two UV pulses separated by 50 ps are measured with the streak camera, with an accumulation over 10^3 shots. Signal to noise ratio of the order of $10^4/1$ is achievable, mainly limited by the dynamic of the 16 bit CCD camera.

C. High sensitivity device with light Intensifier

Due to the quite low detection efficiency of the streak tube (in term of number of output visible photon per incident x-ray photon), a significant amount of incident signal is required even in accumulation mode. For relatively low emis-
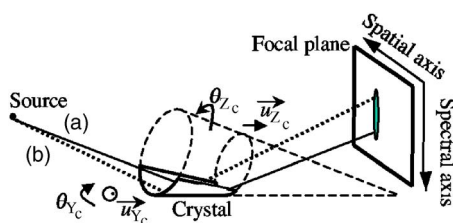
FIG. 11. Sketch of the conical crystal. Two different rays (a) and (b) are presented, corresponding to two different reflected wavelengths according to the Bragg's law.
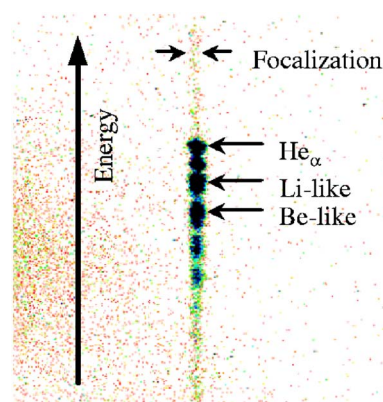

FIG. 12. (Color online). Spectrum of the x-ray emission from laser irradiated Ar clusters recorded at the focal plane of the conical crystal at its best focusing adjustment ($\theta_{Y_C}=0$).

sive sources, the sensibility can be increased, inserting a light intensifier between the streak tube and the CCD camera. We use a pulsed light intensifier realized by Photek corporation. It is basically composed of three elements: an entrance photocathode S20 which converts photons into electrons, a microchannel plates MCP140 which multiplies the electronic signal and an output phosphor screen P43 which converts backelectrons into photons. The electrons created at the photocathode are extracted thanks to a high voltage. Its duration and time delay with the incident signal at the streak entrance have been both optimized. This new apparatus in the measuring chain adds a specific granular noise, essentially due to thermal electrons extracted from the light intensifier photocathode. This extra noise is smoothed with long time accumulation and has no major incidence on our measurements. With this device and high enough gain, all the noises are lower than the signal generated by one single electron inside the streak tube. We should note that the temporal and the spatial resolutions is slightly degraded with this setup due to the 40 μm spatial resolution of the light intensifier.

V. TIME-RESOLVED X-RAY SPECTROSCOPY

A. Conical crystal device

The spectral dispersion is obtained with the use of an x-ray Bragg crystal. In order to maximize the signal collection, crystals with different curvature configurations have been proposed and realized, such as cylindrical, spherical,[34,35] toroidal,[36] or conical crystals.[12,37–39]

Because of the cluttered experimental area, it is easier to set the streak camera along a radius of the experimental chamber, the x-ray source being generated at the center. The conical crystal configuration presents the major advantage to focus the x-ray spectrum on a line perpendicular to the source-detector axis. This line can easily be aligned along the streak camera entrance slit.

For this practical aspect, and in order to collect the maximum number of photons, a relatively large 50×40 mm^2 conical crystal has been used. It has been realized by Saint Gobain Crystals & Detectors corporation. It is composed of potassium acid phtalate with orthorhombic internal arrangement and interplanar parameter of $2d=26.64$ Å . The cone half angle is 0.3 rad with lower and upper radii of curvature of 88.65 and 103.42 mm, respectively. A sketch of the crystal is presented in Fig. 11 with respect to its conical shape (dashed line). The crystal aperture is set to 20 mm width with a filter, in order to limit the effect of the spherical aberration.

The x-ray emission resulting from laser-cluster interaction[40] has been used for spectral calibration. The spectral range corresponding to the He$_\alpha$ line and its satellites (3.05–3.15 keV energy range) has been specifically observed, using second order diffraction of the crystal. We present in Fig. 12 such a spectrum directly measured with a CCD camera on the focal plane. Focusing adjustments are realized with the help of motorized rotation mounts around u_{Y_c} and u_{Z_c} axis (cf. Fig. 11). θ_{Y_C} is mainly responsible for the x-ray spectra focusing, and its origin is set for the best focusing adjustment. The width (along the spatial direction) is then 300 μm FWHM (cf. Fig. 12). That corresponds to the nonlimited x-ray source size in this imaged direction.

In order to give a better account of the focusing, analytical calculations cannot be achieved because of the spherical aberration arising for large crystal aperture. Therefore, a ray tracing code has been performed.[41] Both experimental and calculated focal lines are presented in Fig. 13. The top of the figure presents images recorded at the focal plane for different values of the crystal angle θ_{Y_C}. To get these images, a standard He-Ne laser has been focused on a nail-needle, making a point source similar to a microsize x-ray source. The bottom of the figure presents the calculated evolution of the focused pattern. The code results are in pretty good agreement with the measurements, leading to a minimal width of the order of 100 μm. One can also observe large wings, typical from spherical aberration.

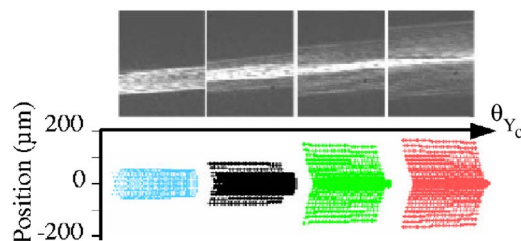The spectral dispersion is presented in Fig. 14, obtained

FIG. 13. (Color online). Focal line obtained with the conical crystal for different values of θ_{Y_C}. From left to right: $\theta_{Y_C}=-0.5$, 0.5, 1.5, and 2.5 mrad. Bottom pictures are obtained from a ray tracing calculation. Top pictures are the corresponding images measured using a He-Ne laser, and with the same scale.
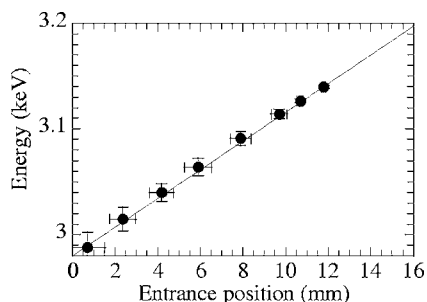
FIG. 14. Spectral dispersion induced by the conical crystal on the plane located at the streak camera entrance. Full circles: experimental results. Full line: calculation.

from both experiments and calculations. The agreement is good, confirming the confidence we can have in calculated predictions. Considering the spectral width observed for the He$_\alpha$ line on Fig. 12 (150 μm FWHM), we get an upper limit of 2 eV for the crystal spectral resolution. That is the dominant contribution of the spectral resolution for time-resolved x-ray spectroscopy, larger than the spatial resolution of the streak camera.

B. Measurement and analysis

The absolute calibration of the laser-irradiated Ar cluster x-ray source[40] has been previously performed with a time-integrated spectrometer.[42] This allows us to estimate the integrated reflectivity of the crystal at 3.14 keV for the second order of diffraction to be $(1.8 \pm 0.8) \times 10^{-5}$ rad, which is consistent with theoretical studies on the same type of crystal.[43]

The spectrum at the focal plane being 300 μm width, one of the major difficulty is to adjust such a signal with the $(93 \pm 10)\mu$m entrance slit of the streak camera. Taking into account this signal loss induced by the crystal-streak coupling, we get the detection threshold for 3.14 keV photons, with the setup including the light intensifier. The detection threshold decreases, inversely proportional to the square root of the number of shots accumulated. Considering 36 000 shots, the detection threshold equals 1.35 x-ray photon per ps, per shot, and per mm^2 on the photocathode surface collection.

A time-resolved x-ray spectrum from laser irradiated cluster is presented in Fig. 15 with KI photocathode. The initial argon cluster radius is 275 Å and the laser energy on

target is 3.5 mJ. The typical emission intensity corresponds to a few 10^5 x-ray photon per electron-volt, per shot, and per steradian[40] (at 3.14 keV). In order to get the time-resolved x-ray spectrum, computational corrections have to be performed. The first one concerns a tilt correction, due to the rotation discrepancy between the streak tube and the CCD camera. Then, both the static and dynamic curvatures have to be corrected on the streaked trace. A new term arises from the crystal temporal dispersion which is purely due to its geometry. The fully corrected image is presented at the bottom of Fig. 15. This is obtained by summing up 360 000 shots at 40 Hz, which represents 2 1/2 hours of nonstop running experiment.

We observe that the He$_\alpha$ and its satellites have a duration shorter than the temporal resolution, evaluated for this result to 1.3 ps rms. That is slightly larger than the $\Delta t = 770 \pm 130$ fs rms previously obtained for accumulation over 10^3 shots, with UV pulse and corresponding Palladium photocathode. The use of KI photocathode should decrease the temporal resolution as reported in Sec. III C. The crystal should degrade it, but within 100 fs, as estimated from previous studies.[35] In the present case, the spatial resolution is lowered by the use of the light intensifier, inducing a major contribution from Δt_{LSF}. The x-ray source duration, in itself, contributes also to enlarge the observed duration. Nevertheless, we believe that this temporal resolution degradation is mainly due to the temporal jitter which results from the very long term laser stability.

VI. DISCUSSION

An extended characterization of a high-dynamic range time-resolved x-ray spectrometer is presented. It is based on the coupling of a conical Bragg crystal with a subpicosecond x-ray streak camera, operated in accumulation mode (with a repetition rate up to 1 kHz).

The performances of the system have been determined with a simple setup using ultrashort UV pulses, focused with a planocylindrical lens. Its dynamic range has been demonstrated to reach up to $10^4/1$, mainly limited by the readout CCD camera. The spatial properties of the streak tube have been determined, in term of spatial resolution (49 ± 9 μm FWHM), collection surface (93 ± 10 μm FWHM width), and trace curvatures. A computational treatment has been developed in order to get the time-resolved x-ray spectra from the recorded images.

The temporal jitter induced by the accumulation mode, is controlled by the use of optical switches that synchronize the sweeping voltage with the incident signal. A temporal resolution of 770 ± 130 fs rms is get for accumulation over more than 10^3 shots. It is mainly limited by the jitter, evaluated at 560 ± 90 fs rms.

A maximum value for the incident signal intensity has been determined, in order to neglect the space charge effect. The insertion of a light intensifier has been studied for low emissive incident signal. The detection threshold is then lowered, limited by the signal generated by a single electron inside the streak tube.

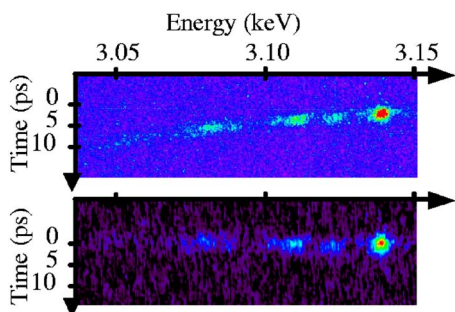The coupling of the conical Bragg crystal with the streak

FIG. 15. (Color online). Time-resolved spectrum of laser irradiated-Ar cluster x-ray emission accumulated over 360 000 shots. Top: without correction. Bottom: with correction. The initial radius of clusters is ~275 Å, and the laser energy on target is 3.5 mJ with a pulse duration of 300 fs FWHM.

tube has been studied. Its spatial focusing and spectral dispersion are well reproduced by ray tracing calculations. A time-resolved x-ray spectrum from laser irradiated cluster is presented, summing up 360 000 shots at 40 Hz. That demonstrates the very long term stability of the device (a few hours), offering a time resolution better than 1.3 ps rms. The spectral resolution of the entire device is better than 2 eV.

ACKNOWLEDGMENTS

[1] K. Sokolowski-Tinten *et al.*, Nature (London) **422**, 287 (2003).
[2] A. Cavalleri *et al.*, Phys. Rev. B **63**, 193306 (2001).
[3] F. Ráksi, K. Wilson, Z. Jiang, A. Ikhlef, C. Côté, and J. C. Kieffer, J. Chem. Phys. **104**, 6066 (1996).
[4] P. Palianov, J. Gaudin, F. Quéré, P. Meynadier, M. Perdrix, and P. Martin, Proc. SPIE **5482**, 21 (2004).
[5] A. Rousse *et al.*, Nature (London) **410**, 65 (2001).
[6] K. Sokolowski-Tinten *et al.*, Phys. Rev. Lett. **87**, 225701 (2001).
[7] R. Shepherd *et al.*, Rev. Sci. Instrum. **66**, 719 (1995).
[8] A. Maksimchuk *et al.*, Rev. Sci. Instrum. **67**, 697 (1996).
[9] P. Gallant *et al.*, Proc. SPIE **3157**, 44 (1997).
[10] V. Losovoi and I. Ushkov, Proc. SPIE **4948**, 297 (2003).
[11] F. Pisani, M. Koenig, D. Batani, T. Hall, D. Desenne, J. Bruneau, and C. Reverdin, Rev. Sci. Instrum. **70**, 3314 (1999).
[12] U. Andiel, K. Eidmann, F. Pisani, K. Witte, I. Uschmann, O. Wehrhan, and E. Förster, Rev. Sci. Instrum. **74**, 2369 (2003).
[13] J. C. Kieffer *et al.*, Phys. Fluids B **5**, 2676 (1993).
[14] P. Audebert *et al.*, Phys. Rev. Lett. **94**, 025004 (2005).
[15] P. Gallant, P. Forget, F. Dorchies, Z. Jiang, and J. C. Kieffer, Rev. Sci. Instrum. **71**, 3627 (2000).
[16] M. Shakya and Z. Chang, Appl. Phys. Lett. **87**, 041103 (2005).
[17] G. Mourou and W. Knox, Appl. Phys. Lett. **35**, 492 (1979).
[18] C. Belzile, J. C. Kieffer, C.-Y. Côté, T. Oksenhendler, and D. Kaplan, Rev. Sci. Instrum. **73**, 1617 (2002).
[19] V. Bagnoud and F. Salin, Appl. Phys. B **70**, (Suppl.), S165 (2000).
[20] H. Liu, J. Yao, and A. Puri, Opt. Commun. **109**, 139 (1994).
[21] P. A. Jaanimagi, D. K. Bradley, J. Duff, G. C. Gregory, and M. C. Richardson, Rev. Sci. Instrum. **59**, 1854 (1988).
[22] P. A. Jaanimagi, A. Mens, and J. Rebuffie, Proc. SPIE **2549**, 62 (1995).
[23] B. Henke, J. Liesegang, and S. Smith, Phys. Rev. B **19**, 3004 (1979).
[24] B. Henke, J. Knauer, and K. Premaratne, J. Appl. Phys. **52**, 1509 (1981).
[25] B. Boutry, C. Cavailler, and N. Fleurot, Proc. SPIE **348**, 766 (1982).
[26] Z. Chang *et al.*, Appl. Phys. Lett. **69**, 133 (1996).
[27] U. Andiel, K. Eidmann, and K. Witte, Phys. Rev. E **63**, 026407 (2001).
[28] T. Oksenhendler, Ph.D. thesis, École Polytechnique, 2004.
[29] H. Niu and W. Sibbett, Rev. Sci. Instrum. **52**, 1830 (1981).
[30] M. Monastyrski, V. Degtyareva, M. Schelev, and V. Tarasov, Nucl. Instrum. Methods Phys. Res. A **427**, 225 (1999).
[31] V. Degtyareva, M. Monastyrsky, M. Schelev, and V. Tarasov, Opt. Eng. **37**, 2227 (1998).
[32] B.-L. Qian and H. Elsayed-Ali, J. Appl. Phys. **91**, 462 (2002).
[33] D. Gontier, A. Mens, P. Millier, and S. Verdelet, Chocs-CEA DAM **21**, 63 (1999).
[34] B. Young *et al.*, Rev. Sci. Instrum. **69**, 4049 (1998).
[35] T. Missalla, I. Uschmann, E. Förster, G. Jenke, and D. von der Linde, Rev. Sci. Instrum. **70**, 1288 (1999).
[36] A. Hauer, J. Kilkenny, and O. Landen, Rev. Sci. Instrum. **56**, 803 (1985).
[37] T. Hall, J. Phys. E **17**, 110 (1984).
[38] R. Marjoribanks, M. Richardson, P. Audebert, D. Bradley, G. Gregory, and P. Jaanimagi, Proc. SPIE **831**, 185 (1987).
[39] E. Martinolli, M. Koenig, J. Boudenne, E. Perelli, D. Batani, and T. Hall, Rev. Sci. Instrum. **75**, 2024 (2004).
[40] F. Dorchies, T. Caillaud, F. Blasco, C. Bonté, H. Jouin, S. Micheau, B. Pons, and J. Stevefelt, Phys. Rev. E **71**, 066410 (2005).
[41] J.-P. Geindre, P. Audebert, V. Nagels, C. Chenais-Popovics, and J.-C. Gauthier, Rapport d'activité, LULI, 2002.
[42] F. Blasco, C. Stenz, F. Salin, A. Faenov, A. Magunov, T. Pikuz, and I. Skobelev, Rev. Sci. Instrum. **72**, 1956 (2001).
[43] A. Burek, Space Sci. Instrum. **2**, 53 (1976).